

ULTRAVIOLET INTERSTELLAR ABSORPTION TOWARD HD 156359, A HALO STAR AT
11 KILOPARSECS IN THE DIRECTION $l = 329^\circ$ AND $b = -15^\circ$ KENNETH R. SEMBACH,¹ BLAIR D. SAVAGE,^{1,2} AND DERCK MASSA^{2,3}

Received 1990 August 6; accepted 1990 October 16

ABSTRACT

UV interstellar absorption line measurements obtained by the *IUE* satellite toward HD 156359 in the direction $l = 328.7$ and $b = -14.5$ are analyzed. We assign HD 156359 an MK classification of O9.7 Ib–II on the basis of UV stellar photospheric and wind lines in its spectrum. The implied spectroscopic distance to HD 156359 is 11.1 kpc, placing it 2.8 kpc below the Galactic plane. By combining five SWP and two LWR spectra we produce a composite spectrum with a signal-to-noise ratio of 15 to 25. The UV interstellar absorption lines of neutral and weakly ionized species (Fe II, Mg II, Si II, S II) sample both dense and tenuous media along the sight line. The strong lines are saturated between -100 km s^{-1} and $+20 \text{ km s}^{-1}$ and reveal a high positive velocity cloud at $+110 \text{ km s}^{-1}$ having an equivalent neutral hydrogen column density of $\log N(\text{H I}) > 17.0$. The highly ionized species (Si IV, C IV, and N V) illustrate the dependence of profile shapes on the effects of Galactic rotation. The Si IV, C IV, and N V profiles extend from -150 km s^{-1} to $+40 \text{ km s}^{-1}$ with half-absorption widths of nearly 100 km s^{-1} . The C IV profiles also exhibit high positive velocity absorption extending from $+40 \text{ km s}^{-1}$ to $+130 \text{ km s}^{-1}$. Such large positive gas velocities are unexpected in the fourth quadrant of the Galaxy. The observed high ionization line profiles are converted into *apparent* optical depth, $\tau_a(v)$, and *apparent* column density, $N_a(v)$, profiles as functions of velocity. Comparison of the $N_a(v)$ profiles between members within each doublet reveals that the observed Si IV and N V profiles are not significantly affected by unresolved saturated structure. The C IV $N_a(v)$ profiles indicate that unresolved saturated structure may be present in the core of each component. The $N_a(v)$ profiles are integrated over velocities between -150 km s^{-1} and $+40 \text{ km s}^{-1}$ to yield total column densities of $\log N = 14.10, 14.77, \text{ and } 14.09$ for Si IV, C IV, and N V, respectively. Kinematical modeling of the high ionization line profiles indicates that a simple model of halo gas corotating with the underlying disk can reproduce the observed line cores but not the high positive velocity C IV absorption. A class of models incorporating a breakdown of corotation at distances between 1.5 and 3.5 kpc away from the Galactic plane reproduces both the cores of the high ionization profiles and the high positive velocity C IV absorption. The detection of N V absorption strongly suggests the presence of gas with a temperature near $2 \times 10^5 \text{ K}$ toward HD 156359. The nonequilibrium cooling of gas in a Galactic fountain can explain the presence of both C IV and N V but falls short by a factor of 5 in producing the required amount of Si IV. Photoionized halo models are able to produce the observed amounts of Si IV and C IV but seem unable to produce sufficient N V. Although composite models are a possibility, the profile similarities for lines of N V, C IV, and Si IV suggests the creation of these ions by a common process.

Subject headings: galaxies: internal motions — interstellar: abundances — stars: individual (HD 156359) — ultraviolet: spectra

1. INTRODUCTION

This paper reports the results of a continuing *International Ultraviolet Explorer (IUE)* program to obtain high-quality ultraviolet interstellar absorption line data for very long path lengths through the interstellar medium of the Galactic disk and low halo. For information about the *IUE* satellite and its spectrographs, see Boggess et al. (1978a, b). We use the observations to study the physical state and kinematics of the halo gas. Differential Galactic rotation effects allow us to probe the Galactic distribution of the different interstellar species accessible to ultraviolet telescopes. The long paths provide large column densities, enabling us to obtain reliable measures of absorption by N V, an important diagnostic of hot collisionally

ionized interstellar gas. The low latitudes ($|b| < 15^\circ$) of the selected sight lines suppress the effects of gas motions perpendicular to the Galactic plane. Thus, line profile shapes are primarily influenced by Galactic rotation, turbulence in the gas, and Galactic radial inflow or outflow.

In our first paper (Savage, Massa, & Sembach 1990), we analyzed the sight line to HD 163522, a star situated beyond the Galactic center at 9.4 kpc in the direction $l = 349.6$ and $b = -9.1$. In that paper we introduced an analysis technique for converting absorption line profiles into *apparent* column densities per unit velocity, $N_a(v)$, and discussed how the observed $N_a(v)$ profiles are expected to behave, given assumptions about the scale height of the species and the Galactic rotation curve for the halo gas. We found that the observed interstellar line profiles for HD 163522 are strongly influenced by Galactic rotation and that the profile shapes are sensitive to the Galactic scale height of the species observed. An analysis of the profiles showed that they did not conform with those expected for the simplest kinematical model, corotating halo gas. However, since the long path to HD 163522 traverses the expanding 3 kpc arm of the Galaxy, such a simple model might

¹ Washburn Observatory, Department of Astronomy, University of Wisconsin-Madison, 475 N, Charter St., Madison, WI 53706.

² Applied Research Corporation, Suite 920, 8201 Corporate Drive, Landover, MD 20785.

³ Guest Observer with the *International Ultraviolet Explorer* satellite, sponsored and operated by the National Aeronautics and Space Administration (USA), by the Science and Engineering Research Council (UK), and by the European Space Agency.

not be expected to be valid. The presence of N v absorption toward HD 163522 with a profile shape similar to those of C iv and Si iv provided fundamental information on the nature of the ionization processes occurring in the halo.

In this paper, we present results based on high-quality multiple *IUE* high-dispersion spectra for the HD 156359 sight line in the direction $l = 328.7$ and $b = -14.5$. Pettini & West (1982) first identified HD 156359 as having a very interesting interstellar absorption line spectrum. In this paper we show that the UV stellar spectrum of HD 156359 is consistent with a MK classification of O9.7 Ib–II. The implied spectroscopic distance of 11.1 kpc places the star 2.8 kpc below the Galactic plane. The brightness and great distance of HD 156359 make it an important star for studying the properties of gas in the low Galactic halo.

In § 2 we report on the UV stellar data for HD 156359. In § 3 we present the UV interstellar line spectrum and in § 4 we discuss our interstellar line analysis techniques. In § 5 we provide an overview of the HD 156359 sight line. In § 6 we model the observed absorption line profiles of the highly ionized gas. In § 7 we discuss the high positive velocity neutral and ionized gas. In § 8 we discuss the origin of the high ion gas seen toward HD 156359. We summarize our results in § 9.

2. THE STELLAR SPECTRUM

HD 156359 was classified O9 III on the basis of photographic spectra obtained by Hill (1970). We have used the additional information contained in the high-dispersion *IUE* UV spectra to assess the accuracy of this classification. Massa (1989) has shown that the strengths of photospheric UV silicon lines are directly related to MK classes for the B stars. Although a similar analysis has not been performed for the O stars, the qualitative progression of various photospheric and

wind lines is obvious in the high UV spectral atlas of O stars compiled by Walborn, Nichols-Bohlin, & Panek (1985). Furthermore, a semiquantitative description of how the wind lines respond to temperature and luminosity is given by Walborn & Nichols-Bohlin (1987). On comparing the UV spectrum of HD 156359 to those contained in the preceding references, it is clear that HD 156359 is cooler and more luminous than an O9 III star.

We searched the *IUE* archives for stars which have spectral types assigned by Walborn near O9 III. Figure 1 compares the spectrum of HD 156359 with those of the O9 III star ι Ori and the O9.7 Ib–II star HD 68450, both Walborn (1972) classifications. The spectra of HD 156359 and HD 68450 are nearly identical and are distinctly different from the spectrum of ι Ori. Notice that the strength of the O iv $\lambda 1342$ multiplet ($\lambda\lambda 1338.6, 1343.0, \text{ and } 1345.5$) is similar in the HD 156359 and HD 68450 spectra but considerably stronger in the ι Ori spectrum. For both HD 156359 and HD 68450 the 1300 Å spectral region is dominated by the distinctive pattern of the Si iii $\lambda 1300$ multiplet ($\lambda\lambda 1294.5, 1296.7, 1298.9, 1301.1, \text{ and } 1303.3$), whereas this multiplet is absent and has been replaced by two strong blends (one probably dominated by N iv $\lambda 1296.6$) in the spectrum of ι Ori. The appearance of the ι Ori spectrum is indicative of all the O9 stars in the Walborn et al. atlas and implies that HD 156359 is an O9.5 or later type star. The Si iv, C iv, and N v wind line profiles of HD 156359 are very similar to those of HD 68450. The similarity of the Si iv profiles is particularly important because they are known to be very luminosity sensitive in O stars (Walborn & Panek 1984).

Based upon these and similar comparisons with the spectra at our disposal, we find that the UV spectrum of HD 68450 is the most suitable match to that of HD 156359. Consequently, we assign HD 156359 a spectral type of O9.7 Ib–II on the basis of its UV spectrum. The difference between our classification

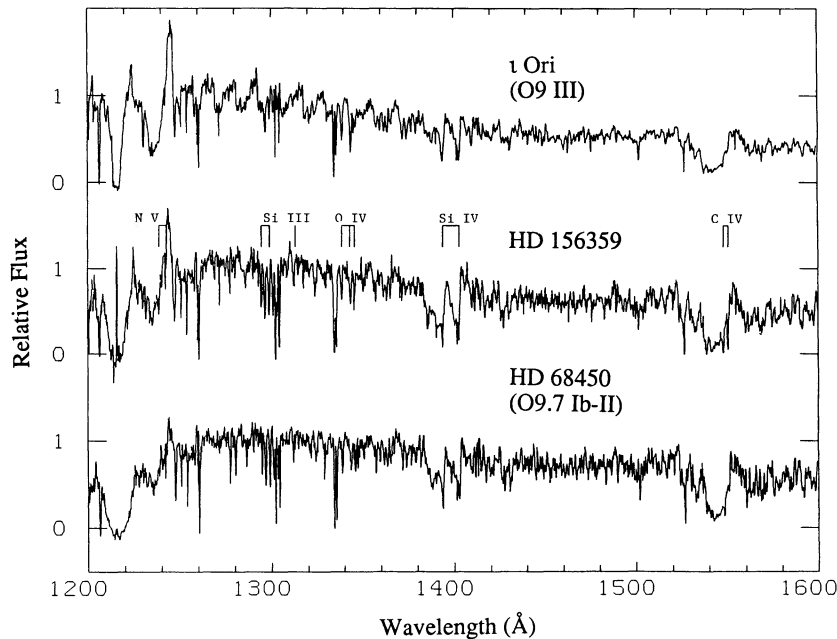


FIG. 1.—Relative flux vs. wavelength in the 1200 to 1600 Å spectral region of ι Ori, HD 156359, and HD 68450. The single high-resolution *IUE* spectra have been smoothed with a 0.25 Å FWHM Gaussian filter. Stellar lines discussed in § 2 of the text are identified above the HD 156359 spectrum. ι Ori and HD 68450 are classified by Walborn (1972) as normal O9 III and O9.7 Ib–II stars, respectively. The UV photospheric and stellar wind features of HD 156359 imply a classification of O9.7 Ib–II.

and Hill's (1970) amounts to roughly a single subclass classification error in the diagonal direction (cooler and more luminous vs. hotter and more compact). Such an error is common in optical classifications made at classification dispersion.

Using our classification, we infer an absolute visual magnitude $M_v \approx -6.0 \pm 0.2$ based upon Walborn's (1973) spectral type $-M_v$ calibration for the O stars. With $m_v = 9.67$, $E(B-V) = 0.14$ (see § 5), and $A_v/E(B-V) = 3.1$ the estimated distance to HD 156359 is 11.1 ± 2.8 kpc, assuming a 25% distance estimate error. This line-of-sight distance corresponds to a galactocentric distance of 5.7 kpc (assuming that the Sun is 8.5 kpc from the Galactic center) and a distance below the Galactic plane of 2.8 kpc. Using Clemens's (1985) Galactic rotation law and assuming that the star is corotating with the disk, the expected LSR radial velocity for HD 156359 is $-59 [+43, -37]$ km s $^{-1}$. The uncertainties on this estimate encompass the observed LSR radial velocity of -89 km s $^{-1}$, corresponding to a kinematic distance of ~ 9.1 kpc, or 18% less than the spectroscopic parallax distance. Although these distance estimates are consistent, the large range of allowable velocities for this sight line prohibits us from obtaining a reliable estimate of the star's peculiar velocity. However, if HD 156359 formed in the Galactic disk it would require a velocity in the $-z$ direction of ~ 300 km s $^{-1}$ to have reached $z = -2.8$ kpc during an estimated lifetime of 10^7 yr.

3. THE INTERSTELLAR SPECTRUM

In order to produce a high-quality (S/N ≈ 15 to 25) spectrum of HD 156359, we obtained multiple *IUE* large-aperture ($10'' \times 20''$) observations of the star to supplement existing archival data. The spectra listed in Table 1 were processed with version 2 of the *IUE* standard spectral processing routines available at the Goddard Space Flight Center (Turnrose & Thompson 1984). For each spectrum the data were corrected for the instrumental background and sensitivity and the echelle blaze function. Since we obtained spectra at various locations in the large aperture, we assumed that the standard processing provided the correct heliocentric velocities for the most recent exposure at the center of the aperture, SWP 35646. These velocities should be accurate to within a 2σ dispersion of 4 km s $^{-1}$

(Thompson, Turnrose, & Bohlin 1982). The other SWP spectra were aligned with SWP 35646 by forcing the strong absorption lines to coincide with each other. A single velocity shift was applied to each spectrum. A comparison of the LWP Fe II lines and the Fe II 1608.456 Å line in the SWP spectra indicated that a velocity shift of -13 km s $^{-1}$ was necessary for each of the LWR spectra. An additional positive background correction of approximately 6%, determined by inspecting the zero-level of nearby saturated interstellar line cores, was applied to those lines shortward of 1300 Å. Cosmic-ray hits were cleaned from several images by replacing the data values of the affected pixels by the average data value of the nearest unaffected pixels. The spectra were linearly interpolated into 5 km s $^{-1}$ bins and added.

We present the relative intensities of selected interstellar lines versus LSR velocity in Figure 2. The LSR velocity correction in the direction of HD 156359 is $v_{\text{LSR}} = v_{\text{helio}} - 0.3$ km s $^{-1}$, assuming a solar speed of $+16.5$ km s $^{-1}$ in the direction $l = 53^\circ$, $b = 25^\circ$ (Mihalas & Binney 1981). The rest wavelengths, f -values, and some comments about the observed absorption are presented in Table 2. The purely photospheric Si III $\lambda 1294.5$ line illustrated in Figure 2 shows the velocity range over which stellar photospheric absorption may be significant. Using this line we estimate a heliocentric radial velocity of -89 km s $^{-1}$ for HD 156359. A ground-based optical radial velocity of -82 km s $^{-1}$ is quoted by Hill (1971), while Pettini & D'Odorico (1986) obtain -72 km s $^{-1}$.

The H I 21 cm emission line data from Heiles & Cleary (1979) for this general sight line is shown in Figure 2 for comparison with the ultraviolet interstellar lines. The 21 cm profile was obtained with the Parkes 60 foot (18 m) telescope centered on $l = 328^\circ.4$ and $b = -14^\circ.4$, $0^\circ.3$ away from HD 156359. The radio data record the average emission over the 48' half-power beam width of the antenna. The total H I column density inferred from the radio data assuming optically thin emission is 8.7×10^{20} atoms cm $^{-2}$. The H I column density inferred from the Ly α line is 5.9×10^{20} atoms cm $^{-2}$ (Savage & Massa 1987). This suggests that either a substantial amount of H I exists beyond the star (which seems unlikely) or that the angular smearing of the radio data has elevated the H I column density above the value seen in absorption.

TABLE 1
HIGH-DISPERSION *IUE* ECHELLE SPECTRA OF HD 156359

Image Number	Exposure Time (min)	Position of Star in Aperture	Velocity Shift ^a (km s $^{-1}$)	Comment
LWR Detector				
4092 ^b	65	Center	-13	
9885 ^b	75	Center	-13	
SWP Detector				
4733 ^b	170	Center	0	Saturation for $\lambda > 1855$ Å
11274 ^b	168	Center	-5	Saturation for $\lambda > 1860$ Å
35646	105	Center	0	
35649	200	$-5''$ offset ^c	+20	Saturation for $\lambda > 1855$ Å
35650	181	$+5''$ offset ^c	-35	Saturation for $\lambda > 1860$ Å

^a The velocity shift applied to each spectrum to bring them into a common heliocentric velocity system is defined by $v_{\text{helio}} = v_{\text{obs}} + \text{velocity shift}$. All spectra were registered with respect to spectrum SWP 35646 for which it was assumed that the standard *IUE* processing provided the correct heliocentric velocity calibration.

^b *IUE* archival data.

^c Spectra were offset $\pm 5''$ along the long axis of the $10'' \times 20''$ aperture in order to reduce the effect of fixed pattern noise in the combined spectrum.

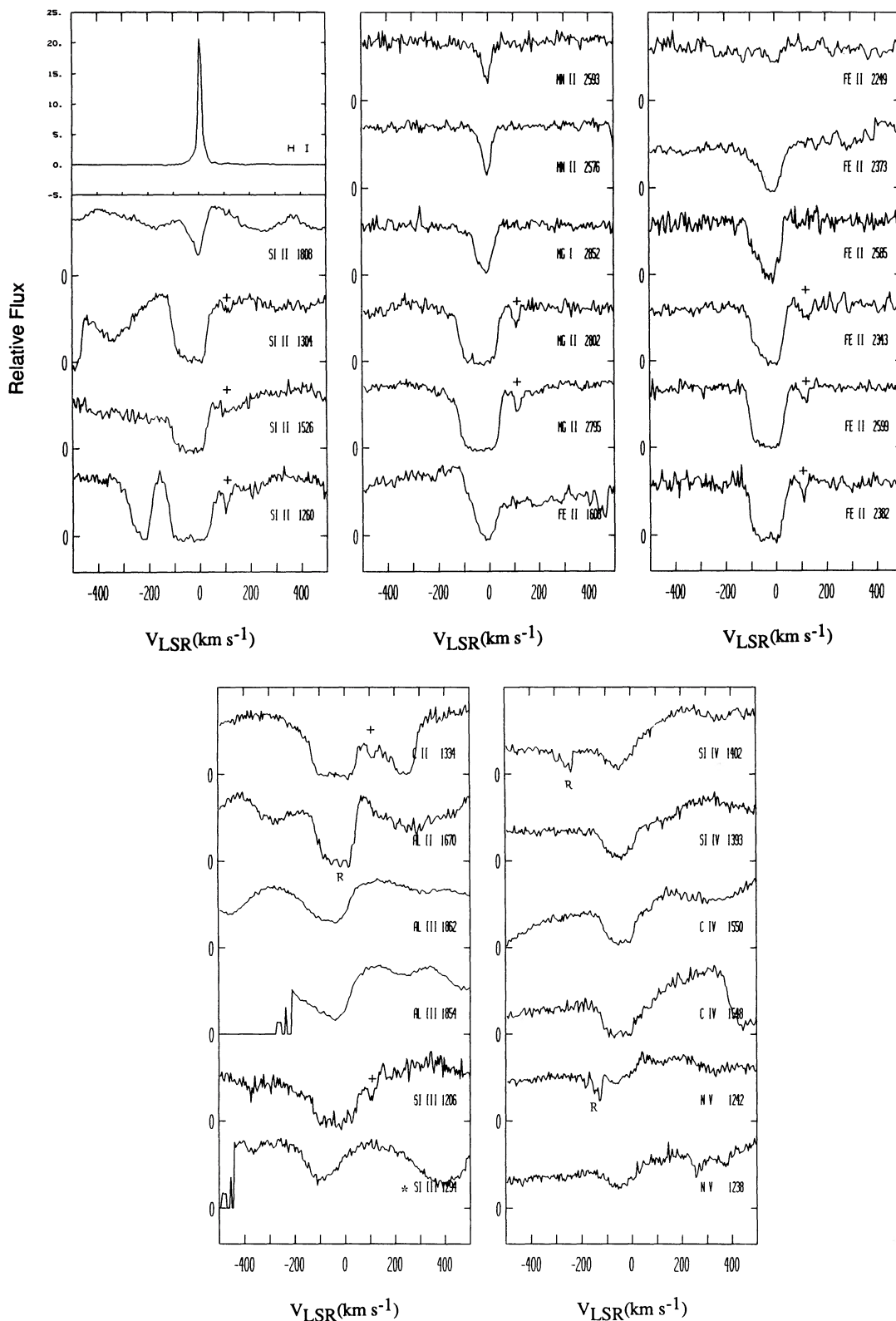


FIG. 2.—Relative flux vs. LSR velocity for the high-resolution UV interstellar lines listed in Table 2. The LSR velocity correction in the direction of HD 156359 is $v_{\text{LSR}} = v_{\text{helio}} - 0.3 \text{ km s}^{-1}$. The profiles shown are the result of co-adding the five SWP or two LWR spectra listed in Table 1. A + symbol above some lines indicates the position of the $+110 \text{ km s}^{-1}$ interstellar feature discussed in § 3 and § 7.2 of the text. R indicates the location of a detector reseau. The photospheric Si III $\lambda 1294.5$ line is illustrated for comparison with the interstellar lines. Note that the interstellar Al III lines are severely blended with the stellar Al III lines, whereas the interstellar lines of Si IV, C IV, and N V occur against relatively smooth stellar P Cygni profiles. The H I 21 cm profile from Heiles & Cleary (1979) shows antenna temperature vs. LSR velocity in the direction $l = 328^\circ 4$ and $b = -14^\circ 4$ and is illustrated for comparison with the UV interstellar lines. The great sensitivity of the UV lines to small amounts of gas is apparent.

TABLE 2
ABSORPTION LINES ILLUSTRATED IN FIGURE 2

Ion	f^a	Wavelength ^b (Å)	Echelle Order	Comment
H I		21 cm		H I 21 cm emission profile is from Heiles & Cleary 1979
Si II	0.0041 ^c	1808.003	76	
Si II	0.100 ^c	1304.369	106	
Si II	0.116 ^c	1526.719	90	
Si II	0.959	1260.418	109	Si II λ 1259.520 appears at $v = -214$ km s ⁻¹
Mn II	0.223	2593.731	89	
Mn II	0.288	2576.107	90	
Mg I	1.77	2852.127	81	
Mg II	0.295	2802.704	82	
Mg II	0.592	2795.528	83	
Fe II	0.062 ^d	1608.456	86	
Fe II	0.0074 ^e	2249.180	103	
Fe II	0.0395	2373.733	97	
Fe II	0.0573	2585.876	89	
Fe II	0.108	2343.495	99	
Fe II	0.203	2599.395	89	
Fe II	0.328	2382.034	97	
C II	0.118	1334.532	103	C II* λ 1335.70 appears at $v = +263$ km s ⁻¹
Al II	1.88	1670.786	83	
Al III	0.268	1862.795	74	Stellar blending renders interstellar line unusable
Al III	0.539	1854.720	74	Stellar blending renders interstellar line unusable
Si III	1.66	1206.510	114	
Si III		1294.54	106	This line from an excited level is a stellar photospheric feature
Si IV	0.262	1402.769	98	
Si IV	0.528	1393.755	99	
C IV	0.097	1550.774	89	Structure in positive velocity wing at $+70$ km s ⁻¹
C IV	0.194	1548.202	89	Saturated core, structure in positive velocity wing at $+70$ km s ⁻¹
N V	0.0757	1242.804	111	
N V	0.152	1238.821	111	Mg II λ 1239.925 appears at $v = +267$ km s ⁻¹

^a f -values are from Morton & Smith (1973) except as noted.

^b Wavelengths are in vacuum for $\lambda < 2000$ Å and in air for $\lambda > 2000$ Å.

^c f -value from Luo, Pradhan, & Shull (1988).

^d f -value from Shull, van Steenberg, & Seab (1983).

^e f -value from Kurucz & Peytremann (1975).

The low ionization lines of Fe II and Si II shown in Figure 2 illustrate the dependence of line shapes on both the high- and low-density phases of the ISM. Lines with small oscillator strengths sample only dense environments within a few hundred parsecs of the Galactic plane, corresponding to distances less than 1 kpc. Consequently, these weak lines tend to be centered near zero velocity. Lines with large oscillator strengths also sample a more extended tenuous medium and as a result are affected by Galactic rotation and turbulence in this medium. The strongest of these lines have cores that are completely saturated between -100 km s⁻¹ and $+20$ km s⁻¹ and wings which extend an additional 20 to 30 km s⁻¹ in either direction.

A high-velocity feature is present in several low ion lines of the interstellar spectrum. The unresolved feature is detected in C II λ 1334, Fe II $\lambda\lambda$ 2343, 2382, and 2599, Mg II $\lambda\lambda$ 2795 and 2802, and Si II $\lambda\lambda$ 1260, 1304, and 1526. It is also detected in the more highly ionized Si III λ 1206 line. The locations of the feature are indicated by a + in Figure 2. The feature has a mean central velocity of $+110$ km s⁻¹ and is typically about 30 km s⁻¹ wide, only slightly broader than the approximate 20 km s⁻¹ resolution of IUE.

Very high signal-to-noise (250:1) and moderate resolution (17 km s⁻¹) ground-based observations of Na I $\lambda\lambda$ 5889.95 and 5895.92 absorption toward HD 156359 are illustrated in

Figure 2 of Pettini & D'Odorico (1986). The Na I absorption reveals three components centered near $v_{\text{LSR}} = 0$, -37 , and -80 km s⁻¹ with line strengths for the D1 line of 140, 52, and 16 mÅ, respectively. A close inspection of our Figure 2 reveals that the weaker lines of Si II, Fe II, and Mn II also exhibit partially resolved component structure extending from the peak absorption at 0 km s⁻¹ to negative velocities. The $+110$ km s⁻¹ feature is not seen in Na I.

The high ionization lines of Si IV $\lambda\lambda$ 1393 and 1402, C IV $\lambda\lambda$ 1548 and 1550, and N V $\lambda\lambda$ 1238 and 1242 are illustrated in Figure 2. Although blending with stellar lines renders the Al III λ 1860 doublet unsuitable for our interstellar investigation, the other high ion lines occur against the relatively smooth continua of stellar P Cygni profiles. Note the clear detection of both N V components of the doublet. The cores of all the high ion lines have similar shapes, with half-maximum intensity velocities of -115 km s⁻¹ and $+15$ km s⁻¹. Of these lines, only the λ 1548 component of C IV approaches zero flux in its core.

Both C IV components exhibit a broad absorption wing extending from $+40$ km s⁻¹ to $+130$ km s⁻¹. They also contain a weak feature approximately 30 km s⁻¹ wide near $+70$ km s⁻¹. Neither the Si IV nor N V doublets show absorption over this range. However, Si IV continuum curvature may mask such a wing, and the weakness of the N V lines makes detection difficult. The $+110$ km s⁻¹ feature seen in the low

ion lines is not seen in the high ion lines. The C IV wings and the $+110 \text{ km s}^{-1}$ low ion feature are discussed in greater detail in § 7.

4. ANALYSIS TECHNIQUES

In this section we present our techniques for converting the data into *apparent* optical depth profiles, calculating equivalent widths, and determining reliable column densities from the *apparent* optical depth profiles.

4.1. The Apparent Optical Depth Technique

The analysis technique we employ to study absorption line profiles has not been commonly used for the study of interstellar absorption lines. The technique involves a careful study of the *apparent* optical depth profiles of the absorption lines and uses empirical techniques for evaluating the degree of unresolved saturated structure in those profiles. Several recent examples of the technique are found in Jenkins et al. (1989), Savage et al. (1989), Savage et al. (1990), and Joseph & Jenkins (1991).

We convert an observed absorption line profile (see Fig. 3) into an *apparent* optical depth profile, $\tau_a(v)$, as a function of velocity according to the relation

$$\tau_a(v) = \ln [I_c(v)/I_{\text{obs}}(v)], \quad (1)$$

where $I_c(v)$ is the estimated continuum intensity at velocity v and $I_{\text{obs}}(v)$ is the observed intensity at v . This $\tau_a(v)$ and the true optical depth, $\tau(v)$, are related according to the relation

$$\tau_a(v) = \ln [1/\{\exp[-\tau(v)] \otimes \text{SF}(\Delta v)\}], \quad (2)$$

where $\text{SF}(\Delta v)$ is the instrumental velocity spread function. For $\tau(v) \ll 1$, note that $\tau_a(v) \approx \tau(v) \otimes \text{SF}(\Delta v)$. Note also that when the line is resolved, $\tau_a(v) \approx \tau(v)$. When either of these special conditions applies, $\tau_a(v)$ can be reliably converted into a column density per unit velocity interval via

$$\log [N_a(v)] = \log \tau_a(v) - \log (f\lambda) + 14.576[\text{atoms cm}^{-2} (\text{km s}^{-1})^{-1}], \quad (3)$$

where λ is the rest wavelength of the absorption in Å and the subscript “a” has been attached to the column density notation to distinguish it from the true column density per unit velocity interval, $N(v)$.

When neither of the above conditions applies, as is the case for the high ion lines discussed in this paper, an assessment of the effects of unresolved saturated structure in the $N_a(v)$ profiles and the validity of equation (3) can be made by comparing the $N_a(v)$ profiles of two or more lines of the same ion differing in the quantity $f\lambda$. If the $N_a(v)$ profiles are similar in appearance, then it is likely that effects of unresolved saturated structure are not large and equation (3) is valid. If, however, the $N_a(v)$ profile of the stronger line lies significantly lower than that of the weaker line, then the effects of unresolved saturated structure are likely important.

4.2. Apparent Optical Depth Profiles for Si IV, C IV, and N V

In Figure 4 we present logarithmic plots of the *apparent* optical depth, $\tau_a(v)$ as a function of LSR velocity for Si IV, C IV, and N V. When $\tau_a(v)$ is small and difficult to measure, we replace the solid lines with + symbols. The points above and below the solid lines and + symbols indicate our 1σ error estimate associated with continuum placement and statistical fluctuations in the data as discussed below. Values of the *apparent* column density per unit velocity interval, $N_a(v)$, are indicated on the right-hand axis of each plot.

We apply the above technique to assess the location and degree of saturation in the Si IV, C IV, and N V profiles. Logarithmic plots of $N_a(v)$ as a function of LSR velocity for the strong component (*solid lines and plus signs*) and the weak component (*dashed lines and open circles*) for these doublets are shown in Figure 5. Figure 5a reveals that within the measurement errors of about 0.1 dex unresolved saturation does not affect the Si IV doublet. The strong component of the C IV doublet shown in Figure 5b is difficult to measure between -95 km s^{-1} and $+5 \text{ km s}^{-1}$ because of its great depth. However, in the velocity range $+40 \text{ km s}^{-1}$ to $+130 \text{ km s}^{-1}$, corresponding to the absorption wing noted in the previous

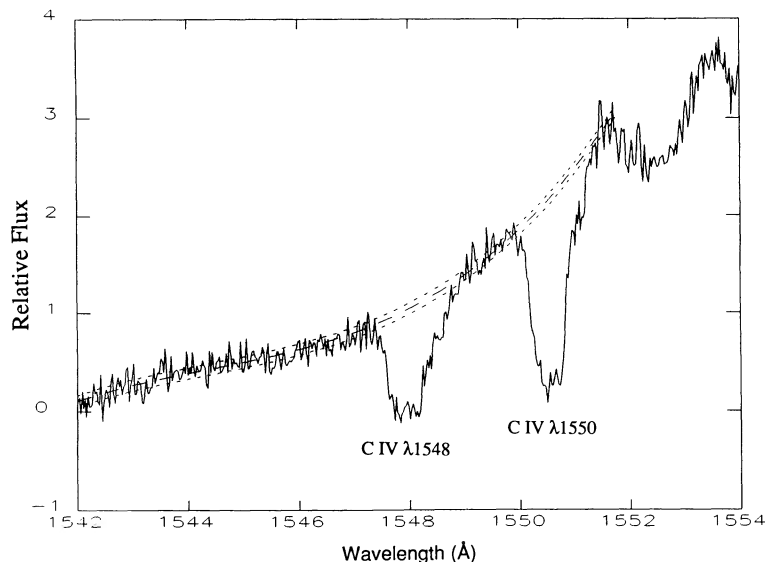


FIG. 3.—Relative flux vs. wavelength for the 1542 to 1554 Å spectral region of HD 156359. The profile shown is the result of co-adding the five SWP spectra listed in Table 1. Notice the smoothly rising stellar P Cygni profile on which the interstellar lines are superposed. The continuum adopted for the C IV doublet is shown as the long dashed line. The associated $\pm 1 \sigma$ continuum placement error bars ($\pm 0.5 \sigma_c$) are shown as short dashed lines.

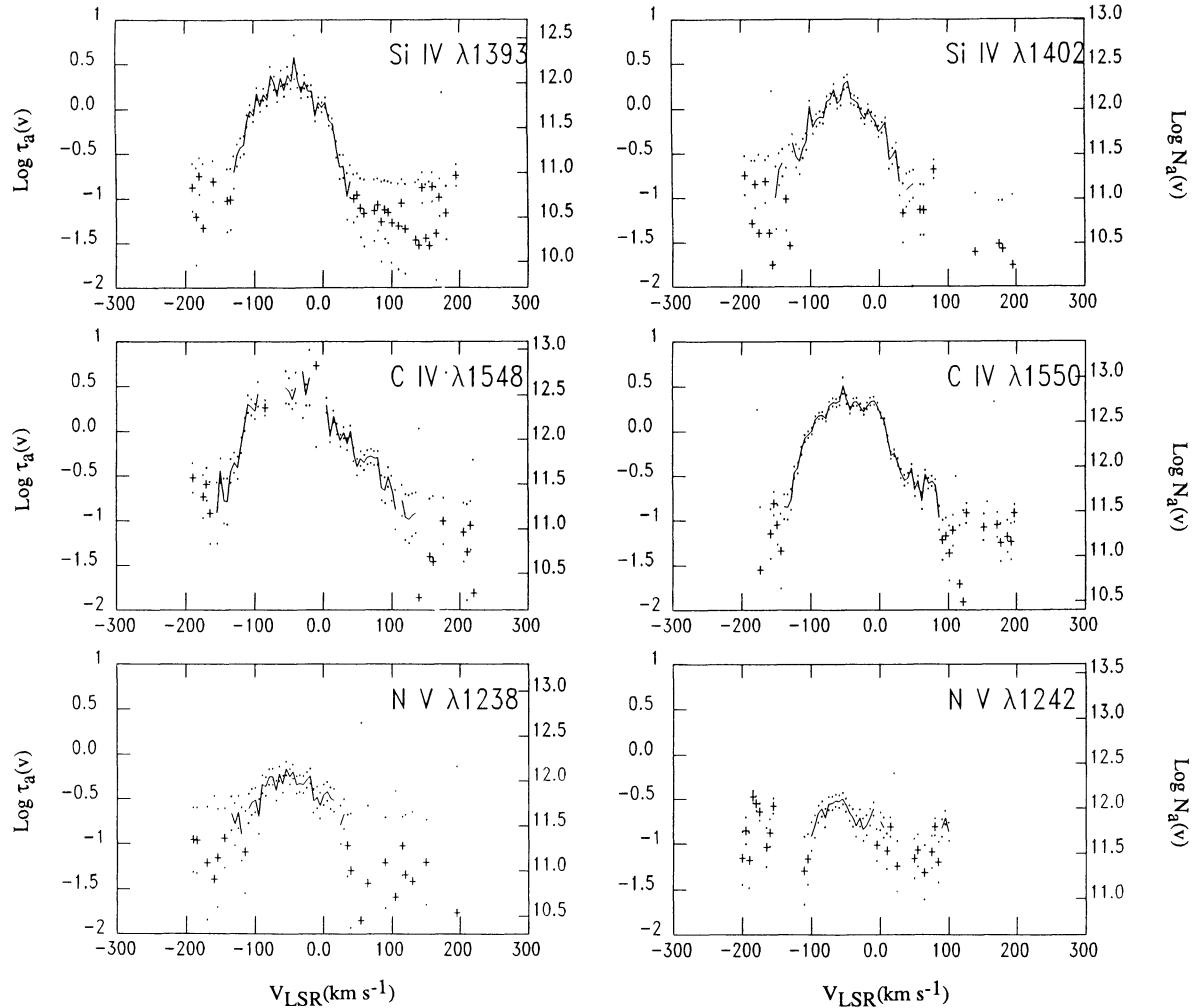


FIG. 4.—Logarithmic plots of *apparent* optical depth, $\tau_a(v)$, vs. LSR velocity for the Si iv, C iv, and N v doublets. The solid lines indicate the *apparent* optical depth, $\tau_a(v)$, constructed from the absorption profiles shown in Fig. 2 as prescribed by eq. (1) in the text. Eq. (3) in the text can be used to relate $\tau_a(v)$ and the *apparent* column density of the species per unit velocity interval, $N_a(v)$. Values of $\log N_a(v)$ are indicated on the right-hand axis of each plot. When $\tau_a(v)$ is very small and difficult to measure, the inferred value is replaced by a + symbol. The noise in the core of the strong C iv $\lambda 1548$ line prevents reliable estimates of $\tau_a(v)$ at those velocities. The dots above and below each solid line or + symbol represent our best estimate of the 1σ errors associated with continuum placement uncertainty and statistical noise fluctuations in the data. R marks the location of a detector reseau that has been omitted when plotting the N v $\lambda 1242$ profile.

section, there is excellent agreement of the C iv profiles. The N v profiles shown in Figure 5c indicate that both components are unsaturated, as expected since this doublet is weak.

The C iv comparison does not yield information concerning saturation in the core of the weak component. The width and general appearance of the line between -150 km s^{-1} and $+40 \text{ km s}^{-1}$ are similar to those of the Si iv doublet and the strong N v line. The C iv $\lambda 1550$ line is approximately the same strength as the stronger Si iv line between -150 km s^{-1} and -25 km s^{-1} and is stronger at velocities greater than -25 km s^{-1} . Therefore, we conclude that saturation may be present in the C iv lines at velocities less than $+40 \text{ km s}^{-1}$ and hence the derived values of $N_a(v)$ at these velocities may be smaller than the values of $N_a(v)$ in the absence of saturation.

4.3. Equivalent Widths and Column Densities

For each high ion line, we selected regions free from obvious stellar contamination, cosmic-rays hits, and reseau marks on both sides of the line, fitted a polynomial (order ≤ 3) to these regions, and calculated the equivalent width. We also calcu-

lated the rms deviation of the continuum, σ_c , about the points in the selected regions on both sides of each line. We chose the error in the equivalent width due to continuum placement to be the error in the equivalent width of the line incurred by raising or lowering the entire continuum by the amount $0.5\sigma_c$. Numerical experiments have shown that this provides a generous estimate of the errors associated with continuum placement, curvature, and assumed functional form. Note that for the very broad interstellar lines we have analyzed, continuum curvature uncertainty strongly contributes to the continuum error. We assumed that the statistical noise fluctuations in the data have an amplitude comparable to σ_c . We added the continuum placement error and the integrated statistical error in quadrature to determine a net error for the equivalent width of each line. Figure 3 illustrates the continuum and associated continuum error bars ($\pm 0.5\sigma_c$) adopted for the C iv doublet.

We list the equivalent widths and their ± 1 errors calculated by the above method for the six high ion lines in Table 3. The error introduced by a 2% zero-level uncertainty is also indicated in parentheses after the 1σ error.

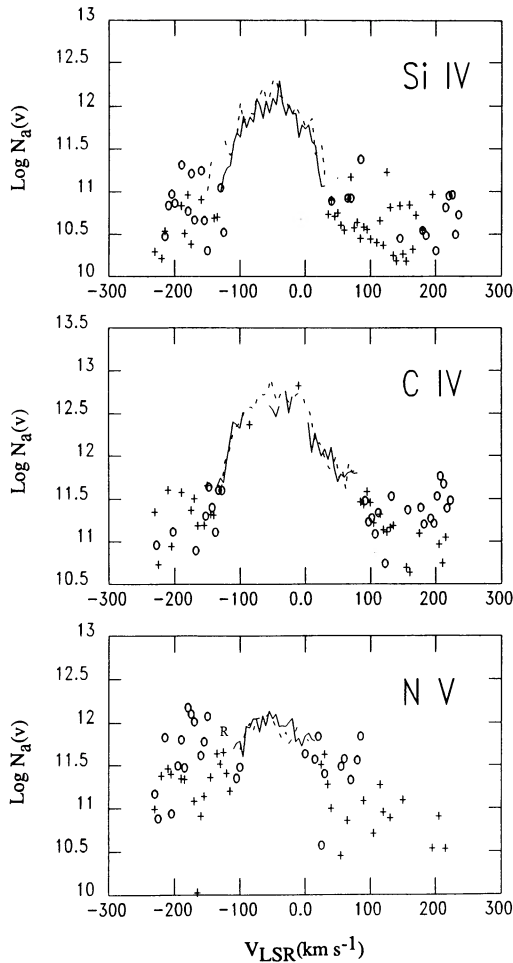


FIG. 5.—Logarithmic comparison plots of *apparent* column density, $N_d(v)$, vs. LSR velocity for the weak (*dashed line*) and strong (*solid line*) components of the Si IV, C IV, and N V doublets. When $N_d(v)$ is very small, the inferred value is replaced by an \circ or $+$ symbol for the weak and strong components, respectively. The similarity of the $N_d(v)$ profiles in the Si IV and N V doublets implies that these lines do not contain unresolved saturated structure. The core of the C IV $\lambda 1548$ line is so strong that portions of it are lost in the noise of the weak signal, preventing an estimate of $N_d(v)$ at certain velocities. The core of the C IV $\lambda 1550$ line may contain unresolved saturated structure. However, the unavailability of the $\lambda 1548$ comparison prevents us from empirically determining if such structure actually exists. The C IV profiles agree well between $+40$ km s^{-1} and $+130$ km s^{-1} , suggesting that this wing region does not contain unresolved saturated structure. The profiles also agree well between -150 km s^{-1} and -100 km s^{-1} . R marks the location of a detector rseau that has been omitted in the N V $\lambda 1242$ $N_d(v)$ profile.

Direct integration of $\tau_a(v)$ profiles shown in Figure 4 which are unaffected by unresolved saturated structure yields reliable column densities according to equation (3) and

$$N = \int N_d(v) dv. \quad (4)$$

We list the integrated column densities for the high ion lines in Table 3. We used the same integration range, -150 km s^{-1} to $+40$ km s^{-1} , for each of the lines to provide an interspecies comparison of individual line strengths. However, it was necessary to adjust the negative velocity limit for the N V $\lambda 1242$ line to prevent inclusion of artificial absorption produced by a detector rseau. We determined a lower limit on the column density of the C IV $\lambda 1548$ line by direct integration after repla-

cing all data values in the core within a 1σ statistical noise fluctuation of the zero-level with the value of that 1σ noise fluctuation. The $\pm 1 \sigma$ integrated column density errors due to continuum uncertainty and statistical noise fluctuations in the data are also listed in Table 3 for each line.

Zero-level uncertainties are an additional source of error in the derived column densities. The error, σ_ϵ , in *apparent* optical depth, $\tau_a(v)$, incurred by a zero-level uncertainty, ϵ , in the normalized line profile is given by

$$\sigma_\epsilon[\tau_a(v)] = \ln[1 + \epsilon e^{\tau_a(v)}]. \quad (5)$$

Clearly, errors in $\tau_a(v)$ as a result of zero-level uncertainties increase with increasing values of $\tau_a(v)$. Assuming $\epsilon = 0.02$ for a 2% zero-point error, a value of $\tau_a = 1$ yields $\sigma_\epsilon[\tau_a(v)] = 0.05$, a 5% error in $\tau_a(v)$. A value of $\tau_a = 3$ yields $\sigma_\epsilon[\tau_a(v)] = 0.34$, an 11% error in $\tau_a(v)$. The error in the integrated column densities for the high ion lines introduced by a 2% zero-level uncertainty is indicated in Table 3 for each line but is not included in the listed $\pm 1 \sigma$ error due to continuum uncertainty and statistical noise fluctuations.

5. PROPERTIES OF THE HD 156359 SIGHT LINE

The HD 156359 sight line ($l = 328^\circ.5$, $b = -14^\circ.5$) extends 11.1 kpc and reaches 2.8 kpc below the Galactic plane. The neutral hydrogen 21 cm survey of Kerr et al. (1986) shows that gas in the underlying disk in the direction of HD 156359 has velocities ranging from -130 km s^{-1} to $+100$ km s^{-1} (their Fig. 4.178). At a latitude of -10° this range is much narrower, -50 km s^{-1} to $+50$ km s^{-1} . Unfortunately, their survey does not extend to the latitude of the star, but it can be seen that the concentration and velocity extent of the H I is decreasing with increasing distance from the plane. The 21 cm emission line data of Heiles & Cleary (1979) presented in Figure 2 supports this claim. This profile is centered at $+7$ km s^{-1} , has full width at half-maximum intensity of 10 km s^{-1} , and contains no significant features at velocities outside a few half widths of the central velocity. The H I column density to the star of 5.9×10^{20} atoms cm^{-2} (Savage & Massa 1987) based on the damped Ly α line implies an average line-of-sight H I density of $n(\text{H I}) = 0.017$ atoms cm^{-3} . Since much of the H I column density is likely produced by relatively local gas close to the Galactic plane, we conclude that most of the HD 156359 sight line penetrates through a very tenuous medium.

The total column density of an exponentially distributed gas along a sight line with latitude b is given by

$$N = n_0 H(1 - e^{-|z|/H})/|\sin b|, \quad (6)$$

where n_0 is the gas midplane density and H is the gas scale height. The disk and halo gas survey of Savage & Massa (1987) indicates that $\langle n_0 \rangle = 2 \times 10^{-9}$, 7×10^{-9} , and 3×10^{-9} atoms cm^{-3} for Si IV, C IV, and N V, respectively. Assuming a scale height of 3 kpc for the gas yields column densities of $\log N = 13.6$, 14.2 , and 13.8 for Si IV, C IV, and N V, respectively. These column densities are factors of 3.2, 3.7, and 1.9 smaller than the observed column densities listed in Table 3, implying that the HD 156359 sight line contains 2–4 times more high ion gas per unit volume than expected for an “average” diffuse sight line in the Savage and Massa sample. This difference may stem from the patchiness of high ion gas in the Galactic disk and halo.

The extinction to HD 156359 is estimated to be $E(B-V) = 0.14$ based upon the observed color, $(B-V) = -0.14$ (Hill 1970), and the intrinsic color, $(B-V)_0 = -0.28$

TABLE 3
COLUMN DENSITIES TOWARD HD 156359^a

ION	WAVELENGTH (Å)	$W_\lambda \pm 1 \sigma$ (mÅ)	$\sigma_{2\%}(W_\lambda)^b$ (mÅ)	LOG N (-1σ)	LOG N_{best}	LOG N ($+1 \sigma$)	$\sigma_{2\%}(N)^b$	INTEGRATION RANGE ^c	
								v_- (km s^{-1})	v_+ (km s^{-1})
Si iv	1393.755	495 ± 20	± 10	13.93	14.04	14.12	± 0.02	-150	+40
Si iv	1402.769	410 ± 24	± 7	14.08	14.15	14.22	± 0.02	-150	+40
C iv	1548.202	771 ± 18	± 14	14.51: ^d	± 0.06	-150	+40
C iv	1548.202	111 ± 16	± 2	13.39	13.52	13.61	± 0.01	+40	+130
C iv	1550.774	599 ± 11	± 12	14.73	14.77	14.82	± 0.02	-150	+40
C iv	1550.774	63 ± 09	± 1	13.44	13.54	13.62	± 0.01	+40	+130
N v	1238.820	207 ± 33	± 4	13.94	14.09	14.20	± 0.01	-150	+40
N v	1238.820	192 ± 26	± 4	13.93	14.06	14.16	± 0.01	-115	+40
N v	1242.804	94 ± 15	± 2	13.88	14.00	14.10	± 0.01	-115	+40

^a Best values and 1σ upper and lower limits for integrated equivalent widths and integrated column densities of the high ionization lines. The column density estimates are based on direct integrations of the *apparent* optical depth profiles shown in Fig. 4 according to eqs. (1) and (3). The $\pm 1 \sigma$ upper and lower limits on W_λ and N include the uncertainty associated with the statistical uncertainty in the data along with the continuum placement uncertainty.

^b Uncertainty introduced in W_λ and N by a zero-level shift equal to 2% of the line depth at line center. This error is not included in the $\pm 1 \sigma$ upper and lower limits quoted on W_λ and N .

^c Two velocity integration ranges are presented for each C iv line, one corresponding to the core of the line and the other corresponding to the positive velocity wing discussed in § 7.1. Two velocity integration ranges are presented for the N v $\lambda 1238$ line, one for comparison with the truncated N v $\lambda 1242$ and the other for comparison with the other high ionization lines. The N v $\lambda 1242$ line integration is truncated at -115 km s^{-1} because of contamination by a nearby reseau on the negative velocity side of the line.

^d Lower limit based upon a direct integration of the C iv $\lambda 1548$ profile shown in Fig. 4 after setting all data values within a 1σ statistical noise fluctuation of the zero level equal to the value of the rms statistical noise fluctuation across the line.

(Johnson 1963), for an O9.7 Ib–II star. This implies the gas-to-dust ratio, $N(\text{H I})/E(B-V)$, for the HD 156359 sight line is $4.2 \times 10^{21} \text{ atoms cm}^{-2} \text{ mag}^{-1}$, somewhat smaller than the local Galactic average of $5.9 \times 10^{21} \text{ atoms cm}^{-2} \text{ mag}^{-1}$ derived from the Copernicus H I and H₂ survey (Bohlin, Savage, & Drake 1978). However, this value of $N(\text{H I})/E(B-V)$ is within the 1σ dispersion of the local measurements.

Several spiral arms are located in the longitudinal direction of HD 156359. The well-defined Sagittarius spiral arm extends from 274° to 32° in longitude as defined by Courtes (1972). Courtes assigns the arm a distance of 1.5 kpc at $l = 330^\circ$ based upon a comparison of H I and H II data. Examination of his Figure 18 reveals that the H II regions in the spiral arm have typical radial velocities of -20 km s^{-1} to -25 km s^{-1} at $l = 330^\circ$. Rickard (1974) finds a peak-to-peak velocity dispersion of 25 km s^{-1} in the Ca II lines of stars associated with the Sagittarius-Carina spiral arm link at $l = 300^\circ$ to 330° . At an in-plane distance of 1.5 kpc, the HD 156359 sight line passes over the Sagittarius arm at an altitude of -400 pc and a line-of-sight velocity of -23 km s^{-1} .

The Norma spiral arm extends from 305° to 333° in longitude (Courtes 1972) and is located at a distance of 3.5 kpc at $l = 330^\circ$. The HD 156359 sight line passes over this arm at an altitude of -900 pc and a line-of-sight velocity of -53 km s^{-1} . The H II regions in this spiral arm have typical radial velocities of $\approx -50 \text{ km s}^{-1}$. Rickard (1974) claims that the radial velocities of the Ca II lines observed over the range $l = 303^\circ$ to 340° are rather constant with a mean value of $\approx -40 \text{ km s}^{-1}$ (his Fig. 7, group C features). He also finds several stars nearer than 3.5 kpc that have Ca II velocities more negative than -70 km s^{-1} , suggesting that there may be peculiar gas motions of $\approx 20 \text{ km s}^{-1}$ if these stars are associated with the Norma spiral arm.

We find no noticeable column density enhancements present in the data at the approximate velocities associated with either the Sagittarius or Norma spiral arms. The tangent point for the

HD 156359 sight line is 4.4 kpc from the Galactic center. Therefore, the data should be unaffected by the 3 kpc expanding arm, which has a galactocentric radius of 3.2 kpc (Oort 1977).

The sight lines in the original survey of Savage & Massa (1987) were chosen to avoid nebulosity, and the field for HD 156359 satisfies this selection criterion. The Galactic non-thermal radio source catalog of Ilovaisky & Lequeux (1972) lists eight supernova remnants satisfying the conditions $325^\circ < l < 333^\circ$ and $b < +1^\circ$. These SNRs have an average diameter of 20 pc and are all centered within 2° of the Galactic plane. The distance estimates for these SNRs are based upon a radio surface brightness–linear diameter relation and range from 4 to 15 kpc. Given these distances, the HD 156359 sight line is always greater than 1 kpc from these SNRs and therefore we expect no contribution to the observed profiles as a result of these objects.

6. KINEMATICAL MODELING OF THE LINE PROFILES

The shapes of the high ion profiles contain information about gas kinematics in the low Galactic halo. The low latitude of the HD 156359 sight line suppresses the effects of gas motions perpendicular to the Galactic plane. There is currently no detailed model of the inner Galaxy to describe radial inflow or outflow of material that might be caused by energetic events in the Galactic center such as those that may have formed the expanding 3 kpc arm of the Galaxy (van der Kruit 1971; Saunders & Pendergast 1984) or by a Galactic fountain of the type described by Bregman (1980) in which $T = 10^6 \text{ K}$ gas rises and moves radially outward, cools ($T < 10^5 \text{ K}$), and returns to the plane moving radially inward. Therefore, we assume that the profile shapes are determined primarily by Galactic rotation effects along the sight line. Figure 6 shows the expected line-of-sight velocity, v_d , as a function of distance, d , toward HD 156359 for halo gas corotating with the underlying disk gas. In

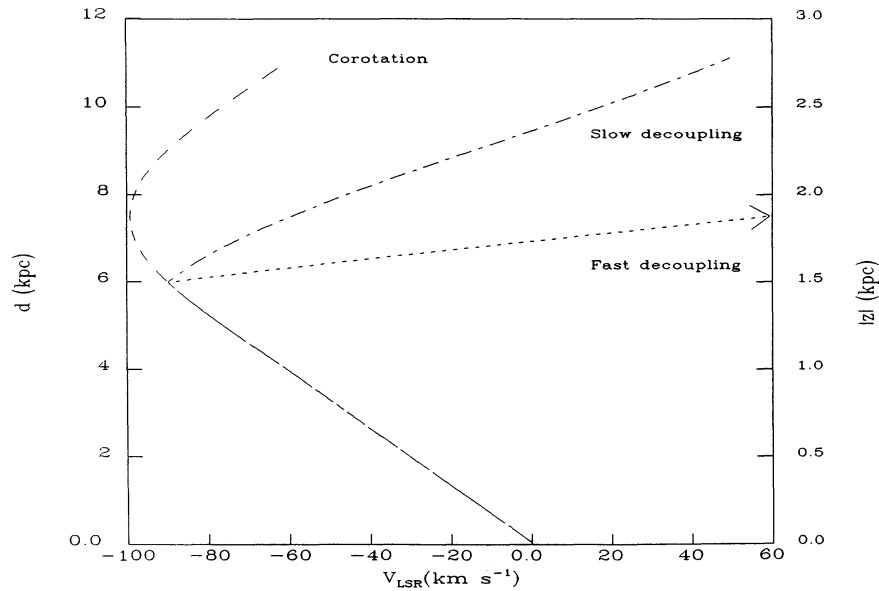


FIG. 6.—LSR radial velocity for gas toward HD 156359 as a function of line-of-sight distance, d (kpc), and distance away from the Galactic plane, $|z|$ (kpc). The long dashed curve depicts gas velocities assuming pure corotation of disk and high z gas and the Galactic rotation curve of Clemens (1985). The dot-dashed curve depicts gas velocities for the base of a “slow decoupling” halo in which deviations from corotation, as defined by $f(|z|)$ (see § 6), set in at $z_i = 1.5$ kpc and corotation ceases completely at $z_f = 3.5$ kpc. The short dashed curve depicts gas velocities for the case of a “fast decoupling” halo in which deviations from corotation set in at $z_i = 1.5$ kpc and corotation ceases completely at $z_f = 2.0$ kpc. The arrow indicates that the velocity of the gas in this case increases to $+111 \text{ km s}^{-1}$ at $d = 8.0$ kpc, remaining constant thereafter.

this direction v_d increases negatively until the tangent point is reached at $d = 7.5$ kpc and increases positively thereafter. The shapes of the observed profiles place constraints on the line-of-sight motions of the gas. In particular, the velocity information contained in the profiles can be used to interpret where along the sight line absorption is occurring, as is done in Galactic studies of the H I 21 cm line.

In this section we introduce the parameters of the simple kinematical model of Savage et al. (1990) and their adopted values for the high ion lines. We examine how varying these parameters influences the shapes of the resulting profiles for this sight line. Once the effects of such variations are understood, we use the model profiles to interpret the observed profiles in terms of the kinematical behavior of the gas.

6.1. Standard Set of Parameters

We adopt a standard set of parameters for our kinematical analysis. For the high ion lines, we choose a gas scale height, H , of 3.0 kpc and an intrinsic gas velocity dispersion, σ , of 30 km s^{-1} . We characterize the rotational behavior of gas in the Galactic disk by Clemens’s (1985) rotation curve with a solar rotational speed of 220 km s^{-1} and solar galactocentric distance of 8.5 kpc. Finally, we specify a function, $f(|z|)$, which relates the rotation of the halo gas to the underlying disk gas as a function of altitude, z , from the Galactic plane. We employ the following functional form of $f(|z|)$ throughout:

$$f(|z|) = \begin{cases} 1.0 & |z| \leq z_i \\ 1.0 - (|z| - z_i)/(z_f - z_i) & z_i < |z| < z_f \\ 0.0 & |z| \geq z_f \end{cases}, \quad (7)$$

where z_i is the altitude at which initial deviations from corotation commence and z_f is the altitude at which corotation ceases completely. For a corotating halo $f(|z|) = 1$ for all values of z . Unless otherwise specified, we have not incorpo-

rated the effects of the 20 km s^{-1} IUE instrumental smearing into our analysis.

6.2. Variation of Model Parameters

Expected column density profiles, $N(v)$, for line-of-sight distances $d = 8.3, 11.1,$ and 13.9 kpc are shown in Figure 7a assuming the standard set of parameters and a corotating halo. Increasing the distance of the star from the $d - 25\%$ limit of 8.3 kpc ($v_d = -96 \text{ km s}^{-1}$) to the nominal distance of 11.1 kpc ($v_d = -59 \text{ km s}^{-1}$) increases absorption at negative velocities and shifts the absorption peak negatively from -52 km s^{-1} to -67 km s^{-1} . Increasing the distance to the $d + 25\%$ limit of 13.9 kpc ($v_d = -16 \text{ km s}^{-1}$) further increases the negative velocity absorption and then shifts the absorption peak velocity positively to -58 km s^{-1} . The negative velocity extent of the profiles is similar in all three cases since the distances are greater than the tangent point distance of 7.5 kpc ($v_d = -99 \text{ km s}^{-1}$). The positive velocity extent is similar in all three cases since $v_d < 0 \text{ km s}^{-1}$ for $d < 15.0$ kpc. The profiles extend beyond -99 km s^{-1} and 0 km s^{-1} because the model contains an intrinsic gas velocity dispersion of 30 km s^{-1} .

Varying the gas scale height of the absorbing ion significantly alters the profile shapes. Figure 7b shows $N(v)$ profiles for the standard model parameters and scale heights $H = 0.3, 1.0,$ and 3.0 kpc. Increasing the scale height increases absorption at negative velocities. For large scale heights, gas at large $|z|$, and thus large d and corresponding v_d , contributes to the absorption.

Changing the velocity dispersion of the gas over moderate ranges results in minor changes in profile width. Employing a disk rotation curve other than that of Clemens (1985), such as a flat rotation curve with a constant linear speed of 220 km s^{-1} , has little effect on the profiles for this sight line. The model is much less sensitive to these parameters than it is to the scale height of the gas.

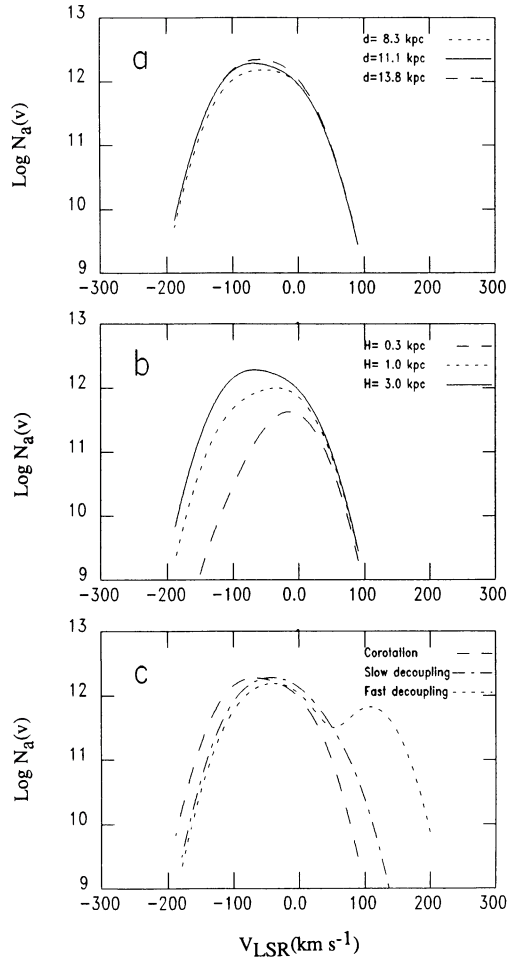


FIG. 7.—(a) Logarithmic comparison plots of *expected* column density per unit velocity interval, $N(v)$, for various line-of-sight distances, d , in the direction of HD 156359. The cases illustrate $N(v)$ vs. v for $d = 11.1, 8.3,$ and 13.8 kpc, corresponding to the nominal distance and distances 25% smaller and larger, respectively. All three cases assume corotating halo gas; a gas scale height, $H = 3.0$ kpc; a gas velocity dispersion, $\sigma = 30$ km s $^{-1}$; and a midplane density, $n_0 = 1 \times 10^{-8}$ atom cm $^{-3}$. (b) Logarithmic comparison plots of *expected* column density per unit velocity interval, $N(v)$, for various gas exponential scale heights, H . The cases illustrate $N(v)$ vs. v for $H = 0.3, 1.0,$ and 3.0 kpc. All three cases assume corotating halo gas; a line-of-sight distance, $d = 11.1$ kpc; a gas velocity dispersion, $\sigma = 30$ km s $^{-1}$; and a midplane density, $n_0 = 1 \times 10^{-8}$ atom cm $^{-3}$. (c) Logarithmic comparison plots of *expected* column density per unit velocity interval, $N(v)$, for various rotating halo models. The cases illustrate $N(v)$ vs. v for a corotating halo (long dashed line), a “slow decoupling” halo (dot-dashed line) with $z_i = 1.5$ kpc and $z_f = 3.5$ kpc, and a “fast decoupling” halo (short dashed line) with $z_i = 1.5$ kpc and $z_f = 2.0$ kpc. All three cases assume the functional form of $f(|z|)$ specified in § 6.1; a line-of-sight distance, $d = 11.1$ kpc; a gas scale height, $H = 3.0$ kpc; a gas velocity dispersion, $\sigma = 30$ km s $^{-1}$; and a midplane density, $n_0 = 1 \times 10^{-8}$ atom cm $^{-3}$.

The most dramatic changes in the expected column density profile occur for models in which deviations from corotation are included. We model deviations from corotation using the functional form of $f(|z|)$ discussed above. Figure 6 illustrates v_d for two cases of deviations from corotation. For this sight line z_i and z_f influence the negative and positive velocity extents of the profile, respectively. Figure 7c illustrates examples of the standard corotating model, a “fast decoupling” model with $z_i = 1.5$ kpc and $z_f = 2.0$ kpc, and a “slow decoupling” model with $z_i = 1.5$ kpc and $z_f = 3.5$ kpc. For

these cases $v_d(11.1 \text{ kpc}) = -59, +111,$ and $+50$ km s $^{-1}$, respectively. In the “fast decoupling” model (short dashed line) the absorption peak shifts to -39 km s $^{-1}$, a broad positive velocity wing forms, and a second peak develops at $+111$ km s $^{-1}$ as a result of gas at $|z| > 2.0$ kpc with no component of motion in the solar direction. The profile for the “slow decoupling” model (dot-dashed line) has a peak absorption at -41 km s $^{-1}$ and a broad positive velocity wing. A second peak never develops in this case because gas along the sight line has an increasingly positive component of motion with respect to the Sun for $d < 14.0$ kpc. For a similar discussion of the effects of deviations from corotation and variation of the model parameters toward HD 163522 ($l = 349^\circ.6, b = -9^\circ.1, d = 9.4$ kpc, $z = -1.5$ kpc) see Savage et al. (1990).

6.3. Comparisons with the Observed Profiles

The high ion profiles presented in Figure 4 can be compared directly to the model profiles described above. To do so, we convolved the model profiles with the *IUE* instrumental function, which we assumed to be a Gaussian with a FWHM of 20 km s $^{-1}$. Figure 8a shows a comparison of the observed Si iv $\lambda 1393$ data (solid line) with the standard corotating model (long dashed line). Since the high ion line cores are very similar, the Si iv data represent their general characteristics. The standard corotating model provides a *general* representation of the observed data between -150 km s $^{-1}$ and $+40$ km s $^{-1}$. However, it considerably overestimates the amount of absorption present between -150 km s $^{-1}$ and -50 km s $^{-1}$. Better fits to the cores of the high ion lines can be obtained with a corotating model by adjusting the model parameters to decrease the amount of gas at large negative velocities. Various combinations of the changing the distance of the star, gas scale height, and gas velocity dispersion increase the quality of the model fit to the high ion line cores.

The “fast decoupling” model shown in Figure 8a (short dashed line) provides an adequate representation of the observed profile cores, but the large amount of positive velocity gas predicted by this model, especially near $+111$ km s $^{-1}$, is not present in any of the observed high ion profiles. The “slow decoupling” model shown in Figure 8a (dot-dashed line) predicts the amount of negative velocity gas seen in the observed profiles more accurately than the standard corotating model, but overestimates the amount of positive velocity gas seen in the Si iv and N v data. However, the “slow decoupling” model is also able to reproduce the positive velocity C iv absorption wing well. Figure 8b shows a comparison of the observed C iv data (solid line) with the “slow decoupling” model (dot-dashed line). The C iv profile is generally well-represented by this model between -150 km s $^{-1}$ and $+130$ km s $^{-1}$. We discuss the observed C iv positive velocity absorption wing further in § 7.

A few general conclusions can be drawn from these comparisons of the observations and model profiles. The standard corotating model adequately describes the high ion cores provided that the input parameters are adjusted so that the amount of gas at large negative velocities is reduced. Several parameters may be adjusted to accomplish this. If the standard corotating model is valid, then either the star is nearer than 11.1 kpc or the scale height of the gas is somewhat less than 3.0 kpc. Notice that decreasing the velocity dispersion of the gas does not improve the quality of the corotating model fit to the data. Although a decrease in the velocity dispersion improves the quality of the fit on the negative velocity side of the line

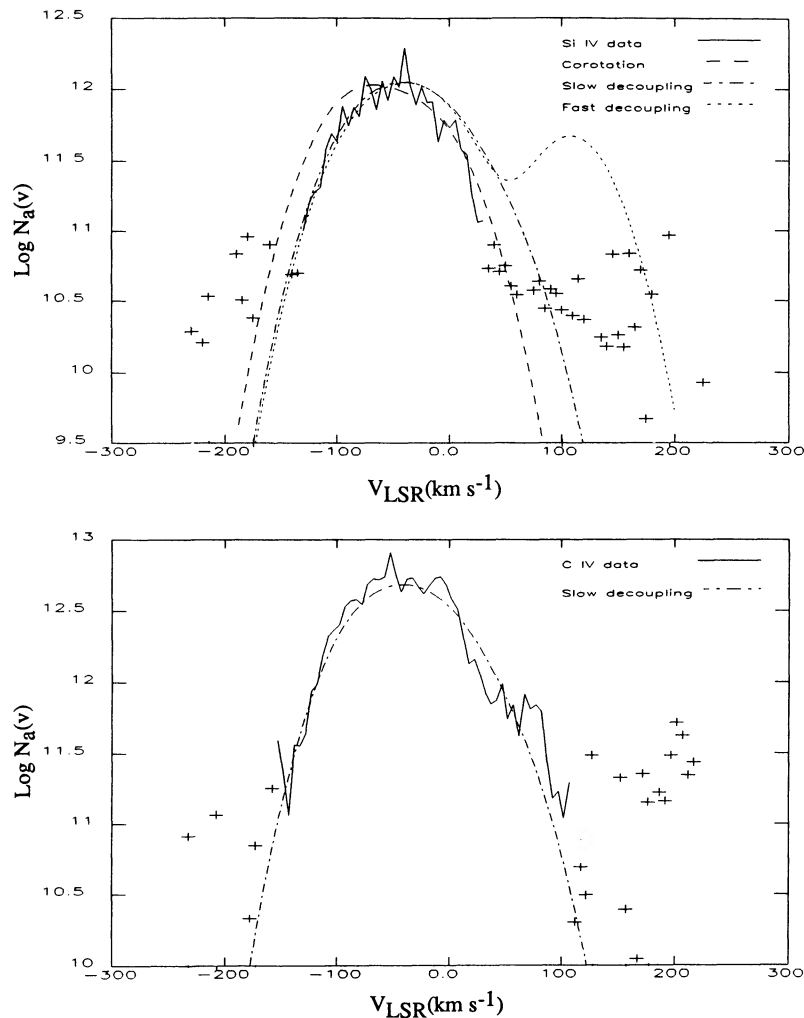


FIG. 8.—(a) Logarithmic comparison plots of *apparent* column density per unit velocity interval, $N_a(v)$ for the observed Si IV $\lambda 1393$ profile of Fig. 4 and the model profiles of Fig. 7c assuming $d = 11.1$ kpc, $H = 3.0$ kpc, $\sigma = 30$ km s $^{-1}$, and midplane densities $n_0 = 5.6 \times 10^{-9}$, 5.8×10^{-9} , and 7.1×10^{-9} atom cm $^{-3}$ for the corotating (long dashed line), “slow decoupling” (dot-dashed line), and “fast decoupling” (short dashed line) halo models, respectively. The model profiles have been converted into *apparent* column density profiles for comparison with the observed data by convolving them with the *IUE* instrumental function, which we assumed to be a Gaussian with FWHM = 20 km s $^{-1}$. The Si IV $\lambda 1393$ line is indicative of all the high ion lines over velocities from -150 km s $^{-1}$ to $+40$ km s $^{-1}$. The corotating model overestimates the amount of high negative velocity gas seen. The “slow decoupling” and “fast decoupling” models adequately describe the core of the Si IV profile but overestimate the amount of positive velocity gas seen. (b) Logarithmic comparison plots of *apparent* column density per unit velocity interval, $N_a(v)$ for the observed C IV $\lambda 1550$ profile of Fig. 4 (solid line and + symbols) and the “slow decoupling” model profile (dot-dashed line) of Fig. 7c assuming a midplane density $n_0 = 2.5 \times 10^{-8}$ atom cm $^{-3}$. The model profile was converted into an *apparent* column density profile for comparison with the observed data by convolving it with the *IUE* instrumental function, which we assumed to be a Gaussian with FWHM = 20 km s $^{-1}$. The “slow decoupling” model adequately describes the entire observed C IV profile, including the positive velocity absorption wings (see § 7) extending from $+40$ km s $^{-1}$ to $+130$ km s $^{-1}$.

cores, it decreases the quality of the fit on the positive velocity side. Note also that no corotating model adequately describes the large positive velocity absorption wing seen in C IV, regardless of how the model parameters are adjusted.

If the C IV absorption wing results from the general gas flow of differential Galactic rotation, then deviations from corotation must be invoked to describe the data. Noncorotating models having $z_i \leq 1.0$ kpc do not provide enough negative velocity gas to represent the high ion line cores. Models having $z_i \approx 1.5$ to 2.0 kpc more accurately describe the high ion profile cores and of these, those with $z_f \approx 3.5$ kpc can reproduce the positive velocity absorption seen in the C IV data. However, they also tend to overestimate the amount of gas at velocities between $+10$ km s $^{-1}$ and $+40$ km s $^{-1}$. Models having steeper decouplings form secondary absorption peaks at $+111$ km s $^{-1}$. Models having more gradual decouplings do not provide

enough absorption at positive velocities to reproduce the C IV wing. Therefore, it appears that a class of noncorotating models with $z_i \approx 1.5$ kpc and $z_f \approx 3.5$ kpc best describes the data for this sight line.

6.4. Comparisons with Other Sight Lines

In our first paper (Savage et al. 1990) we presented results for the sight line to HD 163522, a halo star at a distance of 9.4 kpc in the direction $l = 328^\circ$ and $b = -9^\circ 1'$. In that direction we found that deviations from corotation might be occurring at $d > \sim 6$ kpc ($R = 2.6$ kpc, $z < -1$ kpc), corresponding to regions inside the 3 kpc expanding arm of the Galaxy. The present sight line never passes nearer than the 4.4 kpc from the Galactic center and so our present analysis should not be subject to the same limitations imposed by the absence of high $|z|$ gas (Lockman 1984) within the inner 4 kpc of the Galaxy.

For the HD 163522 sight line we found that a noncorotating model having $z_i = 1.0$ kpc and $z_f = 3.0$ kpc using the standard parameters provided a better fit to the data than a corotating model. Notice that the altitudes where deviations first set in and where corotation ceases completely are larger for the HD 156359 sight line than for the HD 163522 sight line.

Analyses of the sight lines toward Mrk 509 (York et al. 1982) and other extragalactic objects (see York 1982 and references therein) indicate that observed Galactic interstellar line profiles are consistent with corotation up to altitudes as large as 10 kpc. However, these simple analyses examine only the relationship of the velocity extents of the absorption profiles and the velocities expected from a model rotation curve. The analyses do not rule out the possibility of deviations from corotation along these sight lines. In fact, some of the absorption profiles can be better represented by models containing deviations from corotation than they can by a corotating model.

Of the extragalactic sight lines studied, Mrk 509 has the smallest galactocentric radius (~ 5 kpc). For the HD 156359 sight line “slow decoupling” model, we find that deviations from corotation would begin at $R = 4.7$ kpc ($z_i = 1.5$ kpc, $d = 6.0$ kpc, $v_d = -84$ km s $^{-1}$) with corotation ceasing completely near $R = 7.5$ kpc ($z_f = 3.5$ kpc, $d = 13.8$ kpc, $v_d = +111$ km s $^{-1}$). With the limited data available, it appears that if deviations from corotation do exist, they occur within the inner regions of the Galaxy. Comparison of the Galactic sight lines with the extragalactic sight lines suggests that the altitude where these deviations set in, z_i , and the altitude where the halo ceases to rotate, z_f , may be functions of R . We are currently investigating other inner Galaxy sight lines to test the validity of this hypothesis.

7. THE HIGH POSITIVE VELOCITY GAS

In the simplest kinematic model of gas motions in the Galactic halo, that of corotating halo gas discussed in § 6, large positive gas velocities in the direction of HD 156359 are not expected (see Fig. 6). Yet two forms of high positive velocity gas exist along the sight line, the broad absorption wing seen in C iv and the low ion feature at $+110$ km s $^{-1}$, both discussed briefly in § 3.

7.1. The C iv Positive Velocity Absorption Wing

The C iv absorption wing extending from $+40$ km s $^{-1}$ to $+130$ km s $^{-1}$ does not appear to be associated with the star. Figure 3 shows the C iv P Cygni profile of HD 156359. The C iv $\lambda 1548$ wing cannot be formed by the superposition of C iv photospheric features because the stellar C iv wind profiles are very strong and any photospheric components in the $\lambda 1548$ wing region would be “washed out” by the emission portion of the P Cygni profile. The large negative radial velocity of the star (-89 km s $^{-1}$) also minimizes the likelihood of C iv photospheric contamination. Absorption structures seen in the P Cygni profiles of hot stars are often much narrower than the 90 km s $^{-1}$ wide wing and have lifetimes of hours or days (Kaper et al. 1990). The C iv positive velocity wing is seen in spectra taken nearly a decade apart and is unlikely to be associated with stellar wind disturbances. Based on these observations, we are confident in claiming that the positive velocity wing is interstellar.

The C iv absorption wing has a column density of $\log N = 13.53$ over the velocity range from $+40$ km s $^{-1}$ to $+130$ km s $^{-1}$ (Table 3). Note that there is excellent agreement of the apparent column density profiles (see § 4) shown in Figure 5b

between $+40$ km s $^{-1}$ and $+130$ km s $^{-1}$, implying that there is no unresolved saturated structure over this velocity range. The wing is relatively featureless at the resolution of *IUE*, but there is marginally detected structure in the wing at $+70$ km s $^{-1}$.

The decoupling of halo and disk gas at altitudes greater than 1.5 to 2.0 kpc provides a possible explanation for the C iv positive velocity wing (see § 6). Such models reasonably describe both the cores of all the high ion profiles and the positive velocity wings of the C iv profiles. The lack of evidence for high positive velocity absorption wings in Si iv and N v does not invalidate these models. The Si iv P Cygni profile is poorly developed and contains considerable structure making continuum placement in the positive velocity regions of the Si iv lines uncertain. The weakness of the N v lines prevents convincing detection of weak absorption wings in the N v profiles. Higher quality observations than those presented here are needed to determine if the feature is present in these other high ion lines.

7.2. The Low Ion $+110$ km s $^{-1}$ Absorption Feature

The $+110$ km s $^{-1}$ low ion feature is seen in a total of 10 lines of five species. The central velocities and equivalent widths of the detected lines are listed in Table 4. The derived lower limits on the column densities of the five ions listed are based on the equivalent widths of the weakest line in each species and the assumption that these lines are on the linear portion of the curve of growth. Assuming the solar abundances of Allen (1973) and zero depletion for these species yields an internally consistent equivalent neutral hydrogen column density $\log N(\text{H I}) > 17.0$. This column density is lower than the detection limit of the H I data of Heiles & Cleary (1979) shown in Figure 2. The feature is not present in the high signal-to-noise ($\sim 250:1$) Na I data of Pettini & D’Odorico (1986). There is no evidence for this feature in the *IUE* SWP 23529 spectrum of HD 148422 ($l = 329^\circ.9$, $b = -5^\circ.6$, $d = 8.8$ kpc, $z = 0.9$ kpc), possibly indicating that the cloud is either confined to higher latitudes or that the cloud is more distant than 8.8 kpc.

It is unlikely that the low ion feature is associated with the star. The spectral type of O9.7 Ib–II, radial velocity of -89 km s $^{-1}$, and projected rotational velocity of 35 km s $^{-1}$ (Savage & Massa 1987) minimize the possibility that the feature is photospheric. Similarly, the large positive velocity of the feature eliminates the possibility that it is circumstellar given the large mass outflow associated with luminous O stars. Howarth & Prinja (1989) estimate a mass loss rate of $2 \times 10^{-7} M_\odot \text{ yr}^{-1}$ for HD 156359, typical for an O9 star. The feature is seen in spectra taken nearly a decade apart and shows no apparent change in central velocity or strength over this time scale.

A similar high-velocity, low-ion feature was seen in the spectrum of HD 5980 in the SMC by Fitzpatrick & Savage (1983) and was subsequently found to be part of a supernova remnant (Chu & Kennicutt 1988). However, there are no supernova remnants in this direction bright enough at radio wavelengths to be included in the Galactic nonthermal radio source catalog of Ilovaisky & Lequeux (1972), and there is no nebulosity in this direction optically bright enough to be seen on the Palomar Sky Survey plates. Nor is there any trace of the feature in the more highly ionized species of Si iv or C iv, as there is toward HD 5980.

It is possible that the low ion feature is associated with the gas forming the positive velocity C iv wing. The Sun’s component of motion in this direction is $+111$ km s $^{-1}$, implying that the cloud has little or no intrinsic component of motion

along the line of sight. The absorption might be occurring in high-altitude gas that is not corotating with the underlying disk gas. A condensation in the cooling flow associated with gas in the high halo of the inner Galaxy is a possible explanation.

8. THE ORIGIN OF THE HIGHLY IONIZED GAS

The most important result of our study regarding the origin of highly ionized gas in the Galactic disk and halo is the detection of N v absorption in the $\lambda\lambda 1238$ and 1242 lines with optical depth profile cores that are similar to the profile cores for Si iv and C iv. Among the highly ionized species that can be studied by *IUE*, N v is the most difficult to produce by photoionization since the conversion of N iv into N v requires 77 eV and most stellar sources of ionizing radiation have strong 54 eV He⁺ absorption edges. Thus, the N v lines represent the best diagnostic of the hot ISM available in the *IUE* wavelength range. When collisional ionization is in equilibrium with radiative and dielectronic recombination, Si iv, C iv, and N v have peak abundances at temperatures of 0.8×10^5 , 1.0×10^5 , and 2×10^5 K, respectively (Shapiro & Moore 1976). Thus the detection of N v strongly suggests the presence of gas with temperatures near 2×10^5 K.

Theories for the origin of the highly ionized gas found at large distances from the Galactic plane must explain the support and ionization of the gas. Ideas for the support of the gas include cosmic-ray-supported halo models (Hartquist, Pettini, & Tallant 1984; Chevalier & Fransson 1984; Hartquist & Morfill 1986) and Galactic fountain models (Shapiro & Field 1976; Bregman 1980). In some of the cosmic-ray-supported halo models the ionization of the gas is provided by energetic photons from hot white dwarfs, normal Population I stars, or from the extragalactic EUV background. In Galactic fountain models, the ionization is usually associated with cooling collisionally ionized intermediate temperature (0.8 to 3×10^5 K) gas participating in the fountain flow (Edgar & Chevalier 1986).

Detailed calculations have been performed to estimate the expected amounts of Si iv, C iv, and N v in photoionized halo models (Hartquist, Pettini, & Tallant 1984; Chevalier & Fransson 1984; Fransson & Chevalier 1985; Bregman & Harrington 1986). Results from one of these calculations are given

in Table 5 along with values of $N(\text{ion})|\sin b|$ for the average sight line through the halo based on the average results of Savage & Massa (1987), for the Milky Way absorption toward HD 5980 in the SMC (Fitzpatrick & Savage 1983), for HD 163522 beyond the Galactic center (Savage et al. 1990), and for HD 156359. The observed ionic column density of N v toward HD 156359 and the other stars is much greater than predicted by the photoionization calculation listed. While other model calculations differ depending on assumptions about the density distribution of the gas, the spectrum of the ionizing extragalactic background, and whether or not local sources of ionization are included, none of the available models involving realistic conditions for the gas comes within a factor of 10 of the observed N v to C iv abundance ratio. One model that can reproduce the observed C iv to N v ratio is the low-density, $n = 10^{-4} \text{ cm}^{-3}$, model of Bregman & Harrington (1986). However, that model has such a low density and pressure, it is difficult to understand how it might apply to the disk and low halo region sampled along the HD 156359 sight line. In addition, the Bregman and Harrington models include the crucial and very uncertain assumption that the radiation field inferred to exist in the local hot bubble in the energy range from 54 to 500 eV applies everywhere along the sight line. Finally we note that the measures of H α emission associated with high-velocity neutral hydrogen clouds (Kutryev & Reynolds 1989; Songaila, Bryant, & Cowie 1989) have set limits on the flux of hydrogen ionizing radiation escaping from the Galaxy that are up to 30 times smaller than the value adopted in the calculations of Bregman & Harrington (1986). The cooling fountain flow calculations of Edgar & Chevalier (1986) do provide N v and C iv column densities and ionic abundance ratios compatible with the observations for a fountain mass flow rate of about $4 M_{\odot} \text{ yr}^{-1}$ (see Table 5). These same calculations fall short by about a factor of 5 in explaining the observed column density of Si iv and in producing the diffuse C iv emission observed by Martin & Bowyer (1990) toward the Galactic poles. Perhaps a combination of processes (i.e., photoionization and cooling fountain) may be influencing the highly ionized species. However, the similarity of the absorption line profiles for N v, C iv, and Si iv toward HD 156359 (and also HD 163522) suggests that a common process might be responsible for creating all three ions.

The overall amount of intermediate temperature gas toward

TABLE 4
EQUIVALENT WIDTHS FOR THE LOW ION HIGH VELOCITY GAS

Species	Wavelength (Å) ^a	$\langle v \rangle$ (km s ⁻¹)	$W_{\lambda} \pm 1 \sigma$ (mÅ)	Log N^b	Log $N(\text{H I})^c$
C II	1334.532	+112	50 ± 14	>13.43	>16.91
Fe II	2343.495	+125	74 ± 18	>13.15	>17.55
	2599.395	+115	62 ± 15		
	2382.034	+107	59 ± 17		
Mg II	2802.704	+109	80 ± 12	>12.59	>17.17
	2795.528	+114	78 ± 10		
Si II	1304.369	+112	16.6 ± 6	>13.03	>17.51
	1526.719	+109	<30(2 σ)		
	1260.418	+106	27 ± 7		
Si III	1206.510	+106	27 ± 5	>12.10	>16.58

^a Listed in order of increasing f -value within the species.

^b Lower limit based on the measured value of W_{λ} , the f -values in Table 2, and assuming that the weakest line observed in each species is on the linear portion of the curve of growth.

^c Lower limit on $N(\text{H I})$ assuming that the detected feature is produced in a neutral H I region and using the cosmic elemental abundances from Allen (1973) and assuming no gas-phase depletion. In the case of Si III, the limit refers to H⁺.

TABLE 5
COLUMN DENSITIES FOR HIGHLY IONIZED MILKY WAY HALO GAS

Ion	Photoionized Halo ^a $N \sin b $	Cooling Fountain ^b $N \sin b $	Halo Stars ^c $\langle N \sin b \rangle$	HD 5980 ^d $N \sin b $	SN 1987A ^e $N \sin b $	HD 163522 ^f $N \sin b $	HD 156359 ^g $N \sin b $
Al III	4.5×10^{12}	7.3×10^{12}	5.4×10^{12}	...
Si IV	1.3×10^{14}	$(3.3-6.4) \times 10^{12}$	$\approx 2 \times 10^{13}$	2.8×10^{13}	1.9×10^{13}	1.4×10^{13}	3.1×10^{13}
C IV	1.2×10^{14}	$(4.3-7.9) \times 10^{13}$	$\approx 1 \times 10^{14}$	1.8×10^{14}	7.7×10^{13}	5.6×10^{13}	1.5×10^{14}
N V	7.3×10^{11}	$(2.8-3.6) \times 10^{13}$	$\approx 3 \times 10^{13}$	2.2×10^{13}	...	2.1×10^{13}	3.1×10^{13}
O VI	1.4×10^{11}	$(5.8-6.0) \times 10^{14}$	$> 3 \times 10^{13}$

^a Predicted column densities of highly ionized gas through the halo ($N | \sin b |$) based on the cosmic-ray-supported photoionized halo calculations of Hartquist, Pettini, & Tallant (1984). The model values listed are for the model in which warm 10^4 K gas has a large filling factor and a large pressure scale height with $n_0 = 3 \times 10^{-3} \text{ cm}^{-3}$ and $H = 3$ kpc. Note that these photoionized halo models produce very little N v and O vi.

^b Predicted column densities of highly ionized gas through the halo ($N | \sin b |$) on one side of the Galaxy based on the time-dependent ionization calculations of Edgar & Chevalier (1986). The values assume a fountain mass flow rate of $4 M_\odot \text{ yr}^{-1}$ on each side of the Galactic plane. The two values of $N | \sin b |$ listed for each ion involve different assumptions about the sizes of the cooling regions.

^c Observations are from Savage & Massa (1987) for Si IV, C IV, and N v and from Jenkins (1978) for O VI. The value for O VI is listed as a lower limit because the measures extend only to $|z| \approx 1$ kpc.

^d The values listed are for the sight line to HD 5980 in the SMC from Fitzpatrick & Savage (1983) and refer to gas with $v < 100 \text{ km s}^{-1}$.

^e The listed column densities are for gas in the direction of SN 1987A with $v < 120 \text{ km s}^{-1}$ from Savage et al. (1989).

^f The values of $N | \sin b |$ listed for HD 163522 are from Savage, Massa, & Sembach (1990). Values reported measure N to $z = -1.5$ kpc.

^g The values of $N | \sin b |$ listed for HD 156359 are obtained from an average of the values of $N(\text{ion})$ listed in Table 3. Values reported measure N to $z = -2.8$ kpc.

HD 156359 is small. According to the calculations of Shull & van Steenberg (1982), for a plasma in collisional equilibrium with a nitrogen abundance $N/H = 7.9 \times 10^{-5}$ (as revealed through studies of B stars; Pagel & Edmunds 1981), $\sim 6 \times 10^{18}$ atoms cm^{-2} of H^+ near $T = 2 \times 10^5$ K would be required to produce the observed column density of N v listed in Table 3. This represents $\sim 1\%$ of the column of H I seen toward HD 156359 through $\text{Ly}\alpha$ absorption [$N(\text{H I}) = 5.9 \times 10^{20}$ atoms cm^{-2} ; Savage & Massa 1987]. Since 2×10^5 K is near the peak of the cooling function for interstellar gas, we would expect higher and lower temperature gas to be considerably more abundant. Nonequilibrium ionization effects will influence the abundance estimate.

Photoionization models involving extragalactic ionizing radiation predict a large increase in $n(\text{ion})$ for Si IV and C IV near $|z| \approx 1$ kpc (Hartquist et al. 1984; Fransson & Chevalier 1985). In the direction to HD 156359, $z = -1$ kpc occurs at a line-of-sight distance of about 4 kpc. Corotating halo gas at that distance has $v_d = -60 \text{ km s}^{-1}$ according to the velocity lat illustrated in Figure 6. If there were very little Si IV and C IV between the Sun and 4 kpc followed by a substantial increase in $n(\text{Si IV})$ and $n(\text{C IV})$ at that distance we would expect the Si IV and C IV profiles to exhibit sharp maxima near $v = -60 \text{ km s}^{-1}$. Photoionized Si IV and C IV in gas near 10^4 K would have thermal line widths (FWHM) of 4.1 and 6.2 km s^{-1} , respectively. The IUE spectral resolution would smooth such a line to be somewhat broader than the IUE instrumental width (FWHM) of about 20 km s^{-1} . The observed profiles do not contain such narrow structures near -60 km s^{-1} . Instead the lines are very broad with absorption half widths extending from about -115 km s^{-1} to $+15 \text{ km s}^{-1}$. Therefore the density distributions of Si IV and C IV predicted in the simple photoionization model calculations with extragalactic EUV radiation dominating the ionization are incompatible with the observed line profiles. The great breadth of the observed lines and their extension to negative velocities is most easily explained by invoking the effects of Galactic rotation on a gas phase with a substantial mid-plane density and a large scale height (e.g., see the kinematical modeling of § 6).

9. SUMMARY

The primary results of our high-resolution high signal-to-noise study of HD 156359 with the IUE satellite are as follows:

1. We assign HD 156359 a MK spectral type of O9.7 Ib-II based on its UV stellar spectrum. Our classification is slightly different from the O9 III optical classification of Hill (1970). The spectroscopic distance of HD 156359 is 11.1 ± 2.8 kpc, which implies that the star is located 2.8 kpc below the Galactic plane.

2. The high-ionization UV interstellar absorption lines in the UV spectrum of HD 156359 are very broad, with half-maximum intensity velocities of -115 km s^{-1} and $+15 \text{ km s}^{-1}$. We attribute the large breadth and negative velocity extensions of these lines to Galactic rotation operating on a gas phase with a substantial midplane density and a large scale height.

3. The observed high ionization line profiles are converted into *apparent* optical depth profiles, $\tau_a(v)$, and *apparent* column density profiles, $N_a(v)$, as functions of velocity. Comparison of the $N_a(v)$ profiles for lines within each doublet indicates that there is no significant unresolved saturated structure in the Si IV or N v profiles. The cores of the C IV lines may contain unresolved saturated structure. The C IV lines are unaffected by unresolved saturated structure between -100 km s^{-1} and -150 km s^{-1} and between $+40 \text{ km s}^{-1}$ and $+130 \text{ km s}^{-1}$.

4. Direct integration of the $N_a(v)$ profiles for Si IV, C IV, and N v over velocities from -150 km s^{-1} to $+40 \text{ km s}^{-1}$ yields total column densities of $\log N = 14.10, 14.77, \text{ and } 14.09$, respectively. If the N v is produced under conditions of equilibrium collisional ionization in a $T \sim 2 \times 10^5$ K gas having cosmic nitrogen abundances, the implied logarithmic column density of hot ionized gas is 18.8. This can be compared to $\log N(\text{H I}) = 20.77$, based on the strength of the damped $\text{Ly}\alpha$ absorption line (Savage & Massa 1987).

5. The definite detection of N v absorption lines with profile shapes similar to the Si IV and C IV profiles favors a common origin for all three species. These ions might arise in the non-equilibrium cooling of gas in a Galactic fountain. However, the

models predict 5 times less Si IV than is observed. The proper inclusion of photoionization might explain the difference.

6. We find no evidence in the data for an increase in absorption at velocities corresponding to an altitude of 1.0 kpc as is predicted by Si IV and C IV photoionization models involving a postulated extragalactic EUV radiation field (Hartquist et al. 1984; Fransson & Chevalier 1985).

7. Although large positive velocity gas motions are unexpected for the HD 156359 sight line, two forms of high positive velocity gas exist in this direction. Positive velocity absorption wings extending from $+40 \text{ km s}^{-1}$ to $+130 \text{ km s}^{-1}$ are present in the C IV data. The C IV column density of the absorption wing is $\log N = 13.53$. A $+110 \text{ km s}^{-1}$ feature is seen in 10 low ion lines and has an equivalent neutral hydrogen column density of $\log N > 17.0$. We believe that both of these high positive velocity features are interstellar in nature.

8. Our analysis of the observed high ion profile cores indicates that their *general* shapes can be approximated by a simple kinematical model of corotating halo gas under the assumption that the star is nearer than 11.1 kpc and/or the Galactic scale height of the high ion gas is slightly less than 3.0 kpc. However, the observed positive velocity C IV absorption

wings cannot be reproduced by a corotating model, regardless of how the model parameters are adjusted. In order to explain the C IV wings in a kinematical context, deviations from corotation must be invoked. A class of kinematical models having the standard set of parameters discussed in § 6.1 with deviations setting in near $z_i = 1.5 \text{ kpc}$ and a cessation of corotation near $z_f = 3.5 \text{ kpc}$ describes the observed data well. In this situation, the low ion feature near $+110 \text{ km s}^{-1}$ might represent a condensation in the cooling flow associated with gas in the high halo.

We thank the *IUE* observatory staff at the Goddard Space Flight Center for their help in acquiring and processing the *IUE* data for HD 156359. We also thank Ed Jenkins for a careful reading of the manuscript and valuable comments on how to improve it. We acknowledge the use of the SIMBAD data retrieval system of the Centre de Données Astronomiques de Strasbourg. The display and analysis of the spectra were done on the computing facilities of the Midwest Astronomical Data Reduction and Analysis Facility. This work was supported through NASA grants NAG-186 to B. D. S. and NAS 5-29301 to D. M.

REFERENCES

- Allen, C. W. 1973, *Astrophysical Quantities* (3rd ed.; Athlone Press), 31
 Boggess, A., et al. 1978a, *Nature*, 275, 372
 ———. 1978b, *Nature*, 275, 377
 Bohlin, R. C., Savage, B. D., & Drake, J. F. 1978, *ApJ*, 224, 132
 Bregman, J. N. 1980, *ApJ*, 236, 577
 Bregman, J. N., & Harrington, P. J. 1986, *ApJ*, 309, 833
 Chevalier, R. A., & Fransson, C. 1984, *ApJ*, 279, L43
 Chu, Y., & Kennicutt, R. C. 1988, *AJ*, 95, 1111
 Clemens, D. P. 1985, *ApJ*, 295, 422
 Courtes, G. 1972, *Vistas Astr.*, 14, 81
 Edgar, R. J., & Chevalier, R. A. 1986, *ApJ*, 310, L27
 Fransson, C., & Chevalier, R. A. 1985, *ApJ*, 296, 35
 Fitzpatrick, E. L., & Savage, B. D. 1983, *ApJ*, 267, 93
 Hartquist, T. W., & Morfill, G. E. 1986, *ApJ*, 311, 518
 Hartquist, T. W., Pettini, M., & Tallant, A. 1984, *ApJ*, 276, 519
 Heiles, C., & Cleary, M. N. 1979, *Australian J. Phys. Astr. Suppl.*, 47, 1
 Hill, P. W. 1970, *MNRAS*, 150, 23
 ———. 1971, *MemRAS*, 75, 1
 Howarth, I. D., & Prinja, R. K. 1989, *ApJS*, 69, 527
 Ilovaisky, S. A., & Lequeux, J. 1972, *A&A*, 18, 169
 Jenkins, E. B. 1978, *ApJ*, 220, 107
 Jenkins, E. B., Lees, J. A., van Dishoeck, E. F., & Wilcots, E. M. 1989, *ApJ*, 34, 785
 Johnson, H. L. 1963, *Basic Astronomical Data*, ed. K. A. Strand (Chicago: University of Chicago Press), 214
 Joseph, C. L., & Jenkins, E. B. 1991, *ApJ*, 368, 201
 Kaper, L., Heinrichs, H. F., Zwarthoed, G. A. A., & Nichols-Bohlin, J. 1990, in *Proc. NATO Advanced Research Workshop on Angular Momentum and Mass Loss for Hot Stars*, Ames, Iowa, October 23–27, 1989, ed. L. A. Wilson & R. Stalio (Dordrecht: Kluwer), in press
 Kerr, F. J., Bowers, P. F., Jackson, P. D., & Kerr, M. 1986, *A&AS*, 66, 373
 Kurucz, R. L., & Peytremann, E. 1975, *Smithsonian Ap. Obs. Spec. Rept. No.* 362
 Kutuyev, A. S., & Reynolds, R. J. 1989, *ApJ*, 344, L9
 Lockman, F. J. 1984, *ApJ*, 283, 90
 Luo, D., Pradhan, A. K., & Shull, M. J. 1988, *ApJ*, 335, 498
 Martin, S., & Bowyer, C. 1990, *ApJ*, 350, 242
 Massa, D. 1989, *A&A*, 224, 131
 Mihalas, D., & Binney, J. 1981, *Galactic Astronomy* 2d ed.; (San Francisco: Freeman) 399
 Morton, D. C., & Smith, W. H. 1973, *ApJS*, 26, 333
 Oort, J. 1977, *ARAA*, 15, 295
 Pagel, B. E. J., & Edmunds, M. G. 1981, *ARAA*, 19, 77
 Pettini, M., & D'Odorico, S. 1986, *ApJ*, 310, 700
 Pettini, M., & West, K. A. 1982, *ApJ*, 260, 561
 Rickard, L. 1974, *A&A*, 31, 47
 Saunders, R. H., & Pendergast, K. H. 1974, *ApJ*, 188, 489
 Savage, B. D., Jenkins, E. B., Joseph, C. L., & de Boer, K. S. 1989, *ApJ*, 345, 395
 Savage, B. D., & Massa, D. 1987, *ApJ*, 314, 380
 Savage, B. D., Massa, D., & Sembach, K. 1990, *ApJ*, 355, 114
 Shapiro, P. R., & Field, G. B. 1976, *ApJ*, 205, 762
 Shapiro, P. R., & Moore, R. T. 1976, *ApJ*, 207, 406
 Shull, J. M., & van Steenberg, M. E. 1982, *ApJS*, 48, 95
 Shull, J. M., van Steenberg, M. E., & Seab, C. G. 1983, *ApJ*, 271, 408
 Songaila, A., Bryant, W., & Cowie, L. L. 1989, *ApJ*, 345, L71
 Thompson, R. W., Turnrose, B. E., & Bohlin, R. C. 1982, *A&A*, 107, 11
 Turnrose, E. B., & Thompson, R. W. 1984, *IUE Image Processing Information Manual* Version 2.0, (Computer Sci. Corp: TM-84/6058)
 van der Kruit, P. C. 1971, *A&A*, 13, 405
 Walborn, N. R. 1973, *AJ*, 78, 1067
 Walborn, N. R., & Nichols-Bohlin, J. 1987, *PASP*, 99, 40
 Walborn, N. R., Nichols-Bohlin, J., & Panek, R. J. 1985, *International Ultraviolet Explorer Atlas of O-Type Spectra from 1200 to 1900 Å* (NASA Ref. Pub. 1155)
 Walborn, N. R., & Panek, R. J. 1984, *ApJ*, 280, L27
 York, D. G. 1982, *ARAA*, 20, 221
 York, D. G., Blades, J. C., Cowie, L. L., Morton, D. C., Songaila, A., & Wu, C. C. 1982, *ApJ*, 255, 467